# CHAPTER 3

# Topological Insulating Phase in Some Bulk Materials

*We discuss the origin and background of the topological phases and phase transitions in bulk materials in this chapter. Specifically, we will discuss about Half-Heusler compounds and present the results of our investigation on topological insulating nature of LiMgX (X = Bi, Sb, As) in the brackdrop of existing relevant literature. We will discuss the effects of strain fields in realising non-trivial topological nature in such compounds. Also, we discuss different mechanisms by which topological insulating nature can be realised in binary compound such as AuI. The topological phase transitions are qualitatively discussed in terms of the band structures and orbital character inversions which are charactertistic to quantum transitions. This is followed by the quantitative analysis in terms of the $\mathbb{Z}_2$ invariants and angle resolved photo emission spectroscopy-like surface state spectra. These are accompanied with discussions about the stability of the proposed materials in terms of phonon dispersion curves etc.*

## 3.1 The Case of Half-Heusler' LiMgX (X = Bi, Sb, As)

Topological Insulators are a quantum phase of matter known for hosting exotic quantum phenomena such as, spin-momentum locked transport of electrons across the topologically protected surfaces states which are robust against scattering from crystal impurities.[1] Materials

hosting such quantum feature have applications in, spintronics, quantum computation, sensors etc. which has generated enormous interest in the scientific community. Ever since the discovery of topological phenomena in bulk materials (as discussed in chapter 1), numerous materials have been explored theoreticaly as well as experimentally as potential candidates hosting topological insulating nature.[2–7] Various mechanisms have been empolyed in this regard, for example, by applying strain, electric field, doping etc.[8–17]

Application of strain has been a famous choice to realise topological quantum phase transitions in bulk materials for example, $\beta$-$As_2Te_3$, AMgBi (A = Li, Na, K) and elemental tellurium with possibility of hosting multi-functional applications.[14,18–23] In case elemental tellurium which is made up of helical chains governed by three fold screw symmetry and weak van der Waals interaction which can be manipulated by application of pressure to realise non-trivial topological phases.[19] Similarly, AMgBi (A = Li, Na, K) has been investigated to exhibit non-trivial topological properties in Pnma and $P6_3mmc$ phase under the influence of strain. Off these, LiMgBi exhibits type-I anti-ferroelectric properties with polar topological states.[23] In such scenarios where strain induced topological phase transitions are observed in materials, the governing dynamics is that of altered atomic orbitals in the periodic lattice arrangement leading to new hybridizations. Also, apart from the application of strain, in some quintuple layered compounds (such as, $Bi_2Te_3$, $Bi_2Se_3$ etc.) the non-trivial topological character originates intrinsically owing to the strong spin-orbit interactions of the heavy elemets due to high atomic nuclear charge.[24] So the question is, in which other materials can we come across such exotic features? Can we discover/establish a finitely large repository of materials which can exhibit such exotic quantum phenomena for multifunctional applications? These questions directed our focus of first-principles investigations towards Half-Heusler compounds.

It is a well established fact that, the electronic properties of a material originate from the arrangement of atoms in a particular crystal structure governed by space groups. This provides us with innumerable avenues which can be explored wherein, novel materials can be designed and investigated for any desired application. Half-Heusler compounds (of type XYZ) can be aptly described as such materials because, these compounds are made up of $X^+$ ion stuffed in $(YZ)^-$ zincblende sublattice where the elements at X, Y and Z site can be from the *s*, *p* and *d* block of the periodic table.[25] Thus providing enormous permutations and combinations of these elements and hence material properties. Also, the zincblende

sub-lattice of such materials may exhibit band orders across the Fermi level similar to that of bulk HgTe originating through the adiabatic connection of the band topologies.[26] Hence, Half-Heusler compounds are ideal candidates to realise non-trivial topological phases such as topological insulators, apart from properties which can have multi-functional applications such as, semi-conductors, thermoelectrics, piezoelectrics, opto-electronics, superconductivity, magnetism etc.[21,22,27–34] One technique is to employ screening potentials to classify the Half-Heusler compounds into trivial and non-trivial insulators.[35] However, we proceed with application of strain which alters the crystal structure governing electronic properties.

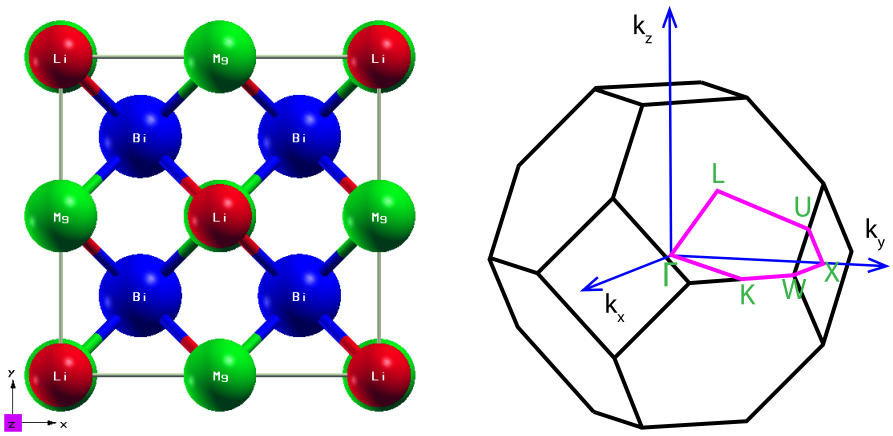


Figure 3.1: Face centered cubic structure of LiMgBi where; Li, Mg and Bi occupy, 4*b*, 4*c* and 4*a* Wyckoff positions respectively (left). Irreducible brillouin zone of the face centered cubic structure indicating the momentum path used for computing electronic band structures and phonon dispersion curves (right).

We began our investigations with Half-Heusler family of LiMgX where the element '*X*' is replaced by Pnictogen family of elements such as, Bi, Sb and As. These systems were previously predicted to be semiconductors due to 8-electron valency of the zincblende sublattice compositions made of MgX (X = Bi, Sb, As).[25] Belonging to the $F\bar{4}3m$ space group these systems are presented in the Hermann-Mauguin representation as [216] (presented in Fig. 3.1). We introduce volume expansion pressure which is similar to hydrostatic pressure but originates from insertion of a cavity nuclei as discussed in the following sections.[37] We observed that, these compounds undergo topological phase transitions under volume expansion pressure which is qualitatively discussed in terms of band dispersion inversions. But, does a band dispersion inversion always gaurantee a non-trivial topological character? We found that, this is not the case and rigorous investigations in terms of $\mathbb{Z}_2$ invariants is

required to compliment the qualitative picture. Also, we observe that, the pressures required for topological phase transitions in such bulk materials is quite high, which motivated us to explore the dimensional engieering of two dimensional phase cleaved from [111] crystal direction of these bulk compounds wherein, the quantum confinement effects may exhibit contrasting scenarios, hosting interesting non-trivial character. We employ, state-of-the-art density functional theory calculations to qualitatively investigate topological phase transitions in half-heusler compounds LiMgX (X = Bi, Sb, As) in terms of electronic structure and orbital projected density of states. These are complimented by computing the topological properties such as $\mathbb{Z}_2$, angle resolved photoemission spectroscopy-like surface state plots using the exact tight-binding hamiltonian generated using maximally localised wannier functions.

## LiMgBi: Structure and Lattice Dynamics

The structure of LiMgBi was optimized under generalised gradient approximation with lattice constant (a) of 6.81 Å which was found to be in agreement with the experimental (6.74 Å) and theoretical (6.71 Å) values.[21] This face centered cubic structure is defined by space group the $F\bar{4}3m$[216] space group which is presented alongside the brillouin zone in Fig. 3.1. The system was found to be dynamically stable (as evident from the phonon dispersion curves presented in Fig. 3.2) with the primitive cell vectors in terms of lattice constant (a) defined as, $v_1 = (a/2)(-1,0,1)$, $v_2 = (a/2)(0,1,1)$, $v_3 = (a/2)(-1,1,0)$ wherein, atoms Li, Mg and Bi occupy, 4*b*, 4*c* and 4*a* Wyckoff positions respectively.[30]

We performed phonon dispersion calculations to verify the lattice dynamic stability of LiMgBi. This is essential because, phonon dynamics are fundamental in underpinning the vibrational lattice dynamics during phase transition and to assertain experimental feasibility of the material. The phonon dispersions of LiMgBi are presented in Fig 3.3 in the absence of volume expansion pressure, indicating dynamic stability and absence of imaginary modes. The three atoms in the unit cell give rise to nine phonon branches in

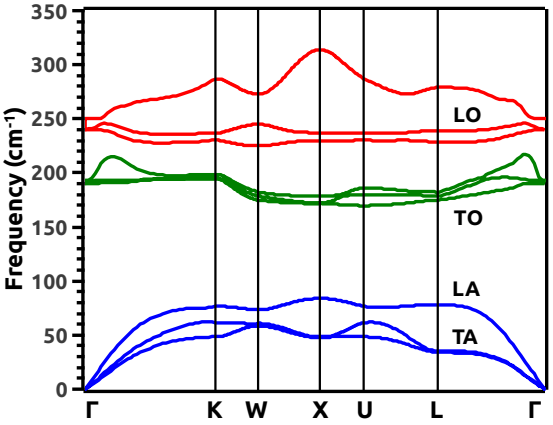


Figure 3.2: Phonon dispersion curves in absence of volume expansion pressure.

the dispersion relation. In lower frequency regime, the three vibrational modes correspond to acoustic branches i.e., one longitudinal acoustic and two transverse acoustic modes which are degenerate along, W → X and L → Γ path in the brillouin zone.[38] Similarly, in higher frequency regime, the six vibrational modes correspond to optical branches i.e., two longitudinal optical and four transverse optical modes. Here, the former is degenerate at Γ and the latter is degenerate along, Γ → K, K → X and X → Γ path in the brillouin zone.[38]

## LiMgBi: Electronic Properties

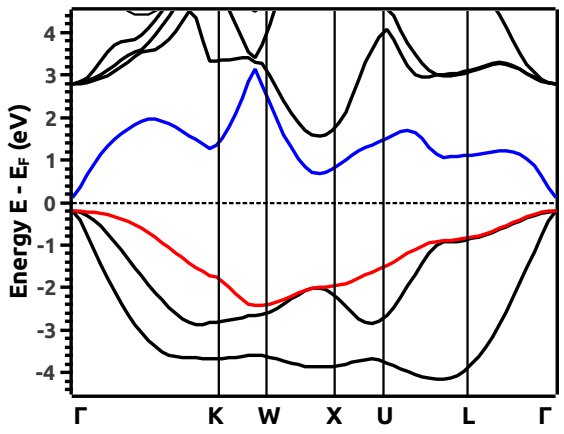


Figure 3.3: Electronic band structure of LiMgBi at in absence of volume expansion pressure.

As expected, due to 8-electron valency, this structure exhibits semi-conducting character as evident from the electronic band structure presented in Fig. 3.3 which was compared to previous reports as presented in Tab. 3.1.[21] Since it is known that, the error in band-gap prediction under generalised gradient approximation is higher as compared to hybrid methods such as HSE06, we performed HSE06 calculations and present them in Tab. 3.1 which indicates that, the results are in strong agreement with previous studies at 0.0% strain and accurate as compared to the generalised gradient approach.

We increased the lattice constant in steps of 0.5% from 0.0% to 8.0% to observe topological quantum phase transitions in LiMgBi. Due to cubic symmetry such increment in lattice gives rise to an isotropic effect which we refer to as the volume expansion pressure. Experimentally, such phenomena can be expected due to the presence of an intrinsic *void* in the crystal, extreme internal *thermal* and *cavitation* pressure arising from impurities known as *cavity nuclei*.

Table 3.1: Theoretical and experimental values of lattice constant (a) and energy band gap.

| Parameter | Work | LiMgBi |
|---|---|---|
| Lattice (Å) | GGA$^{(present)}$ | 6.81 |
| | Theory[21] | 6.71 |
| | Experiment[21,39] | 6.74 |
| Band Gap (eV) | GGA$^{(present)}$ | 0.35 |
| | HSE06$^{(present)}$ | 0.70 |
| | Theory[21] | 0.62 |

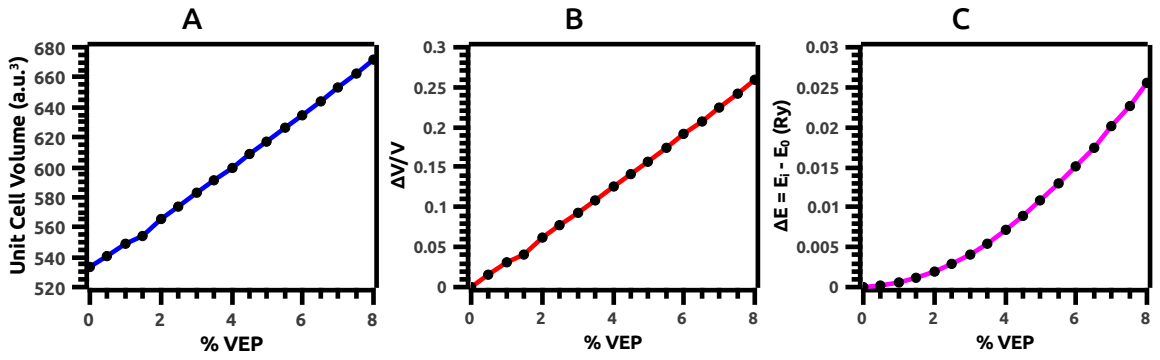


Figure 3.4: (A) Increment in the unit cell volume (a.u.$^3$) due to volume expansion pressure. (B) Volume strain with respect to % volume expansion pressure. (C) Change in total energy (eV) of the system indicating a shift from the equilibrium state leading to a quantum phase transition.

We studied the increment in unit cell volume (a.u.$^3$) under volume expansion pressure (as presented in Fig 3.4(A)) it in terms of, volume strain (presented in Fig 3.4(B)) and, total energy ($\Delta E = E_i$ - $E_0$ in eV) with respect to % volume expansion pressure (presented in Fig 3.4(C)) and found that, due to increment in volume expansion pressure, the system deviates from its equilibrium state which probably would lead to a topological quantum phase transition, analysed quantitatively below.

The analysis of electronic band dispersion gives qualitative insights into the topological quantum phase transitons in materials. We hence, analysed the electronic band structures of LiMgBi and look for inversion in dispersion (under band engineering due to pressure) which characterises the topological insulating nature of the material. We observed that, such a phenomena occurs in LiMgBi at a critical pressure of 4.0% wherein, the system undergoes a phase transition from a semi-conductor to a Dirac semi-metal such that, further application pressure breaks the Dirac degeneracy as presented in Fig. 3.5.

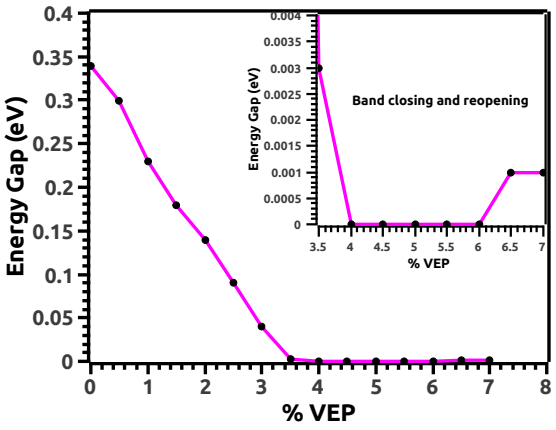


Figure 3.5: The closing and reopening of the band gap with respect to % VEP indicating the Topological Phase Transition in FCC LiMgBi.

In the absence of volume expansion pressure, by generalised gradient approximation and hybrid functional approach, we observed an electronic band gap of 0.35 eV and 0.70 eV respectively at the center of brillouin zone (i.e., at Γ point) as presented in Fig. 3.6(A) and

Tab. 3.1. For qualitative analysis, we performed calculation of the electronic properties such as band gap under generalised gradient approximation and hybrid approach at different volume expansivon pressures of 0%, 4% and 6.5%. We observed that, the energy gap varies as, 0.35 eV → 0.00 eV → 0.001 eV (under generalised gradient approximation) and 0.70 eV → 0.00 eV → 0.04 eV (under hybrid approach); confirming the phenomena of band closing and reopening as observed in Fig. 3.5.

It was observed that, the valence band maxima is doubly degenerate whereas, the conduction band minima is non-degenerate state at the brillouin zone center (Γ). This band feature is protected by two-fold symmetry of the face centered cubic structure. As we gradually increased the volume expansion pressure, at 4.0% critical point, LiMgBi undergoes a topological quantum phase transition from a trivial insulator to a Dirac semimetal (as presented in Fig 3.6(middle)) with degenerate conduction and valence band frontiers. Here, we chose to represent the eigen states at the brillouin zone center (Γ) as $\Gamma_i$ where '$i$' is the band index without spin degeneracy. Figure 3.6 presents the electronic band evolution at the brillouin zone center during the topological quantum phase transition with increase in volume expansion pressure. At 0% pressure the band order is $\Gamma_{10} > \Gamma_8 > \Gamma_6$ where, $\Gamma_{6,8}$ are populated by the $p$-orbitals and $\Gamma_{10}$ is populated by the $s$-orbital with, $\Gamma_{6,8}$ being degenerate as evident from in Fig 3.6(top). With increase in volume expansion pressure, a Dirac degeneracy appears at 4.0% as presented in Fig 3.6(middle) creating degenerate $\Gamma_{8,10}$ bands.

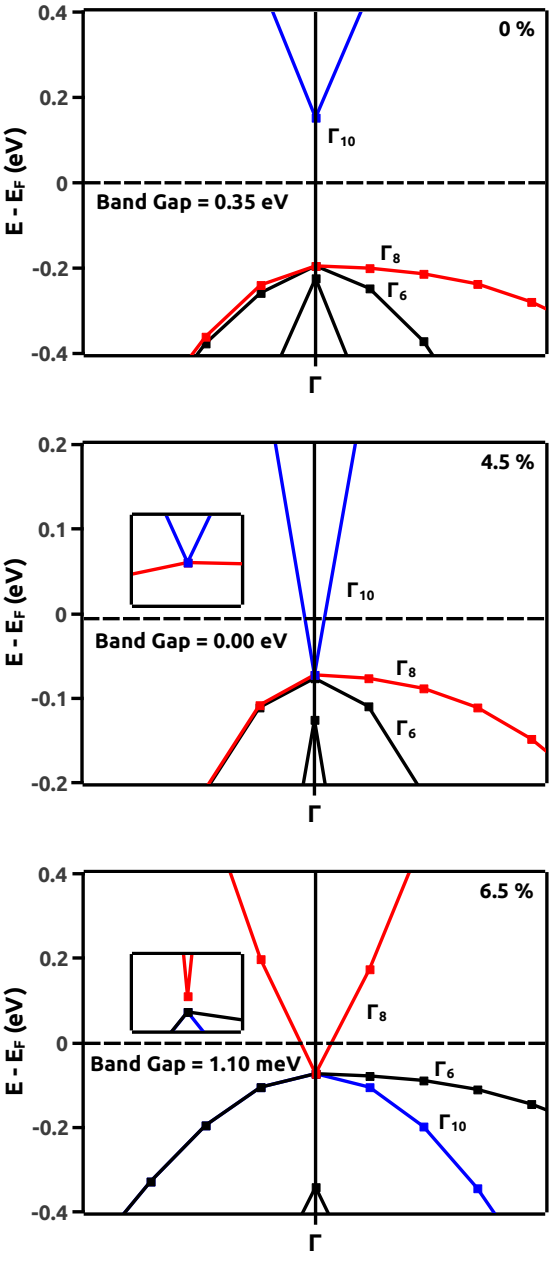


Figure 3.6: Electronic band structure of LiMgBi at, 0.0% (top), 4.5% (middle) and 6.5% (bottom) volume expansion pressure

As this degeneracy forms, the degeneracy of $\Gamma_{6,8}$ lifts off. On further increasing the pressure, the Dirac dispersion is retained till 6% volume expansion pressure beyond which, the band-gap reopens to 1.10 meV (under generalised gradient approximation) as presented in Fig. 3.6(bottom). This reopening indicates towards band inversion in terms of the inverted band order i.e., $\Gamma_8 > \Gamma_6 > \Gamma_{10}$. In order to assertain the non-trivial topological character, we computed the orbital projected density of states.

Figure 3.7(A) presents the orbital projected density of states for LiMgBi at 0% volume expansion pressure. It is clearly evident that, the valence band is populated by the *p*-orbital of Bi while, the conduction band is dominated by the *s*-orbitals of Li, Mg and Bi wherein, a strong hybridization was observed between the *s*-orbitals of Mg and Bi. With increment in pressure, the *s*-orbital contributions of Li, Mg and Bi from conduction band enter the valence band, while the *p*-orbital contribution of Bi from the valence band enters the conduction band at the critical pressure of 4% (as presented in Fig. 3.7(B)). Further increase in pressure makes the hybridization of *s*-orbitals of Mg and Bi weaker while, the hybridization between the *s*-orbitals of Li and Bi become stronger evident from Fig 3.7(C). Thus, at 6.5% of pressure, although the gap opens but, the inverted orbital contributions don't change. Therefore, Fig. 3.7(A-C) visualy summarises the exchange of orbital character due to volume expansion pressure driving the system LiMgBi; through a topological quantum

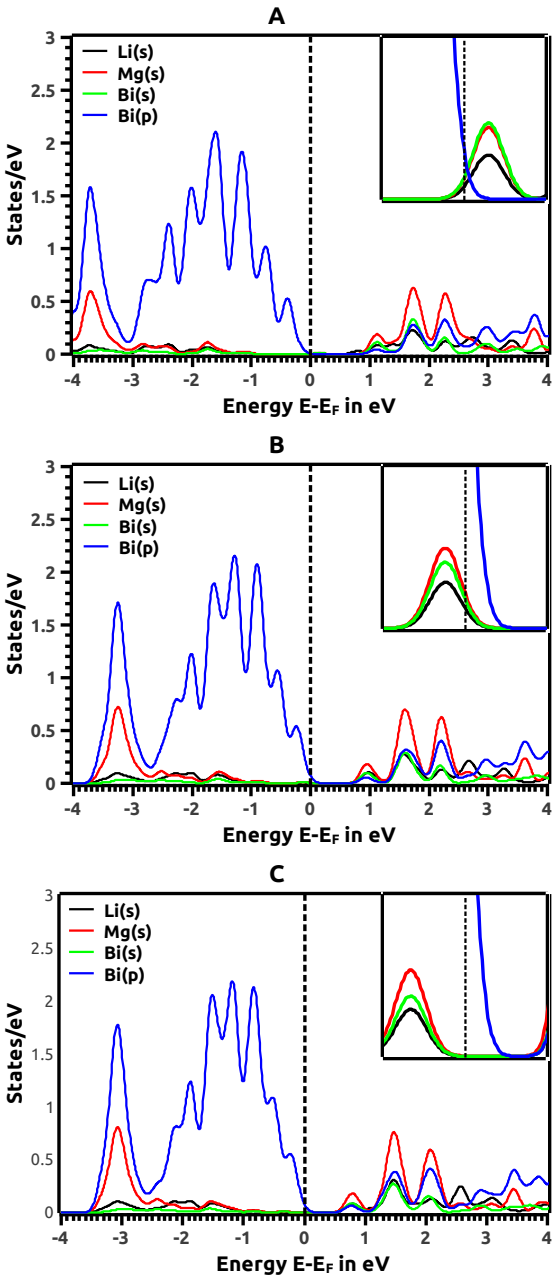


Figure 3.7: Orbital projected density of states at, (A) 0%, (B) 4% and (C) 6.5% volume expansion pressure (inset panels represent states near Fermi level with energy range −0.5 eV to 0.5 eV).

phase transition. We confirm the generalised gradient approximation results in terms of the hybrid approach. Figure 3.8 presents the density of states under hybrid functional approach. It is interesting to note that, similar to the calculations under generalised gradient approximations, the hybrid approach give similar results i.e., at 4% pressure the density of states is semi-metallic and at 6.5% the gap reopens to 40 meV.

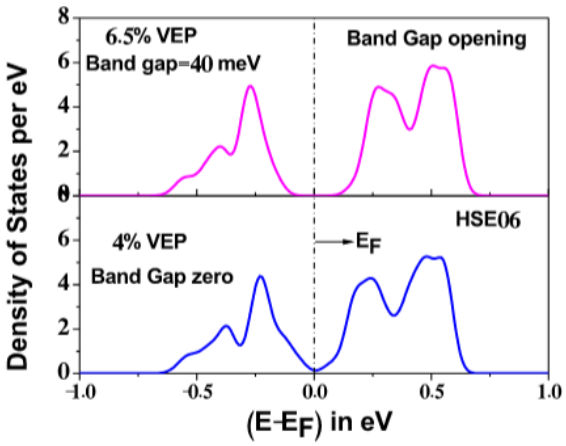


Figure 3.8: Density of states under hybrid approach at 4% and 6.5% volume expansion pressure.

We expected that, the presence of Bi at 4*a* Wyckoff position in the face centered cubic structure would lead to pronounced spin-orbit interactions. Figure 3.8(A) and (B) represent the electronic band structures without and with spin-orbit interactions at critical volume expansion pressure of 4%. The Dirac degeneracy at the brillouin zone center lifts off due to strong spin-orbit interactions giving rise to a band gap of 1.20 meV. This further confirms the characteristic behaviour of a typical topological insulator governed by the relativistic effects which arise from the core electronic contribution of Bi atoms. Since, the gap opening is quite small it indicates that, for spintronic applications, the system has to me maintained at low temperatures.

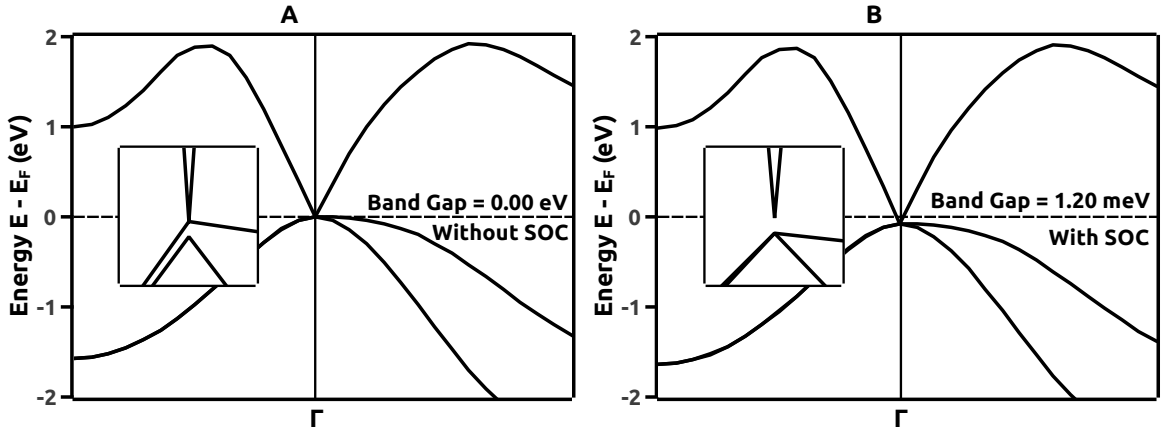


Figure 3.9: Electronic Band Structure at center of the brillouin zone, (**A**) without and (**B**) with spin-orbit interactions, at critical volume expansion pressure of 4%.

## LiMgBi: Topological Properties

Following the investigations of the electronic properties, we computed the non-trivial surface states to quantitatively assertain the topological insulating nature. Figure 3.10 was the angle resolved photo emission spectroscopy-like spectra which clearly indicates the Dirac dispersion of surface states at 4.5% volume expansion pressure i.e., beyond the critical value of pressure. These surface states host dissipationless Fermions which are spin locked with momentum in the brillouin zone. Hence, we can esperimentally verify the non-trivial topological nature of LiMgBi by performing angle resolved photo emission spectroscopy to probe the surface states along the surface.

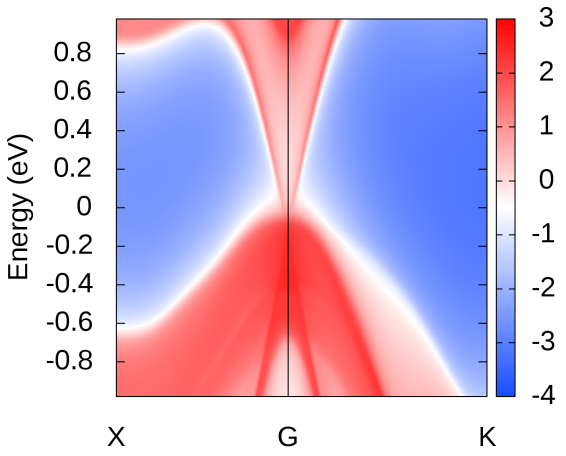


Figure 3.10: Surface states at 4.5% volume expansion pressure.

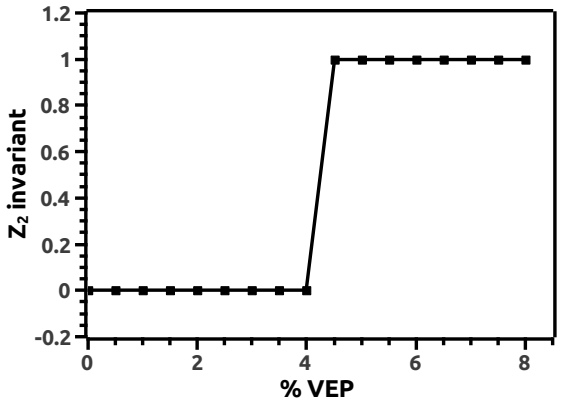


Figure 3.11: Evolution of the $\mathbb{Z}_2$ invariant ($\nu_0$) as a function of pressure.

Apart from the surface states, mathematically, $\mathbb{Z}_2$ invariants are essential to characterize and classify a bulk material as a non-trivial topological insulator. Since, LiMgBi is a half-heusler compound, it does not possess inversion symmetry. Hence, we cannot proceed with Fu and Kane method of computing the $\mathbb{Z}_2$ invariants. We rather use the wannier charge center method discussed in the methodology chapter 2 to compute the $\mathbb{Z}_2$ invariants along six time reversal invariant planes. The computed $\mathbb{Z}_2$ invariants are, $(\nu_0, \nu_1\nu_2\nu_3) = (1, 000)$ indicating that, LiMgBi is a strong topological insulator with robust surface states which won't decompose into two dimensional quantum spin Hall material.[40] In Fig. 3.11 we present the evolution of $\mathbb{Z}_2$ invariant ($\nu_0$) as a function of volume expansion pressure which clearly demarcates the topological quantum phase transitions.

On similar line of investigation (i.e., qualitative and quantitative approach), we explored LiMgSb and LiMgAs. It was expected that, these materials won't be as strong as topological

insulator LiMgBi; owing to the weaker spin-orbit interaction. Motivating us to explore the low dimensional phases of materials. Also, one issue with LiMgBi is that, the Fermi level does not lie in the global gap due to spin-orbit interaction. This motivated us to approach other method such as breaking the crystal symmetry etc.

## LiMgSb and LiMgAs: Structure and Lattice Dynamics

The bulk structures of LiMgSb and LiMgAs exist in face-centered cubic phase with lattice constant (a) under generalised gradient approximation as 6.63 Å and 6.19 Å respectively.[21,22] Here, Wyckoff positions 4*b*, 4*c* and 4*a* are occupied by Li, Mg and Sb / As respectively. The lattice constants presented here are in agreement with previous reports. The interatomic distances in LiMgAs are, As-Mg = 2.69 Å, Mg-Li = 5.38 Å and in LiMgSb are, Sb-Mg = 2.87 Å and Mg-Li = 2.86 Å. We provide greater focus and emphasis on LiMgAs rather than LiMgSb since the former has been well explored and investigated experimentally for various applications.

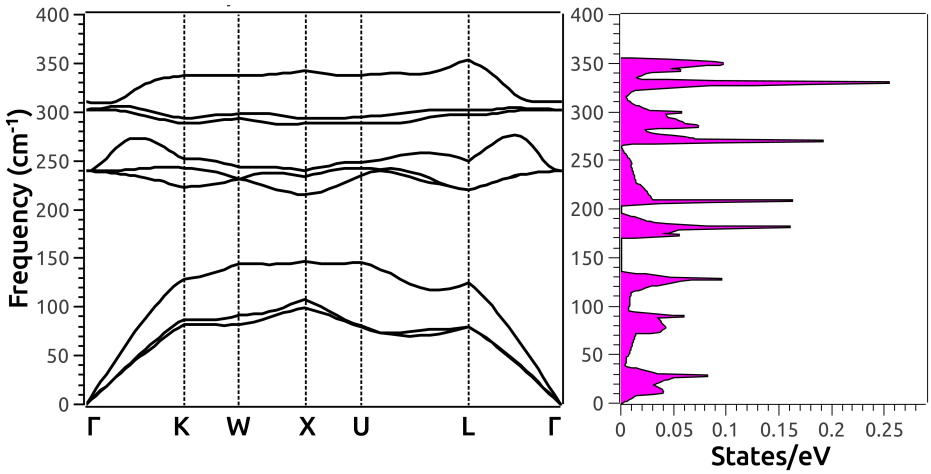


Figure 3.12: Phonon dispersion curves alongside phonon density of states of LiMgAs indicating dynamic stability of the system.

To reiterate the significance of dynamic stability of LiMgAs, we compute the phonon dispresion curves and phonon densiy of states (presented in Fig. 3.12) which clearly indicates the absence of imaginary modes in the entire brillouin zone. The absence of imaginary modes in the phonon dispersions indicates that, the increase in potential energy against any combination of atomic displacements is same as the condition that all phonons have real frequencies in harmonic approximation.[41–45] On the other hand, the presence of imaginary modes indicates that the system is dynamically unstable due to decrease in potential energy

around the equilibrium atomic positions orginating from different combinations of atomic displacements. The phonon dispersion curves and density of states are presented in Fig. 3.12 are under pristine conditions i.e., without any external pressure. Similar to LiMgBi, the three atoms occupying the unit cell give rise to nine phonon branches evident from the dispersion relation which can be decomposed into three in plane acoustic branches dominating lower frequencies and six optical branches dominanting higher frequencies.

## LiMgSb and LiMgAs: Electronic Properties

This face centered cubic structure of LiMgSb hosts indirect band gap of $\sim 0.9$ eV indicating the semi-conducting nature due to 8-electron valency in the absence of volume expansion pressure. Similar to LiMgBi, we apply volume espansion pressure expecting topological quantum phase transitions. As the pressure is applied the indirect gap transforms into a direct gap under 5% volume expansion pressure at the brillouin zone center. At very high pressure of 17% a Dirac degeneracy is observed at the brillouin zone center (as presented in Fig. 3.13(top)) beyond which the gap reopens to 3.1 meV (under 20% pressure as presented in Fig. (bottom)). Such dispersion behaviour is also accompanied with inversion of the $-s$ and $-p$ orbital characters in valence band and conduction band across Fermi level (based on the analysis of orbital projected density of states). However, the non-trivial band dispersions and density of states, the phase transition observed in LiMgSb are further confirmed by computing the topological properties.

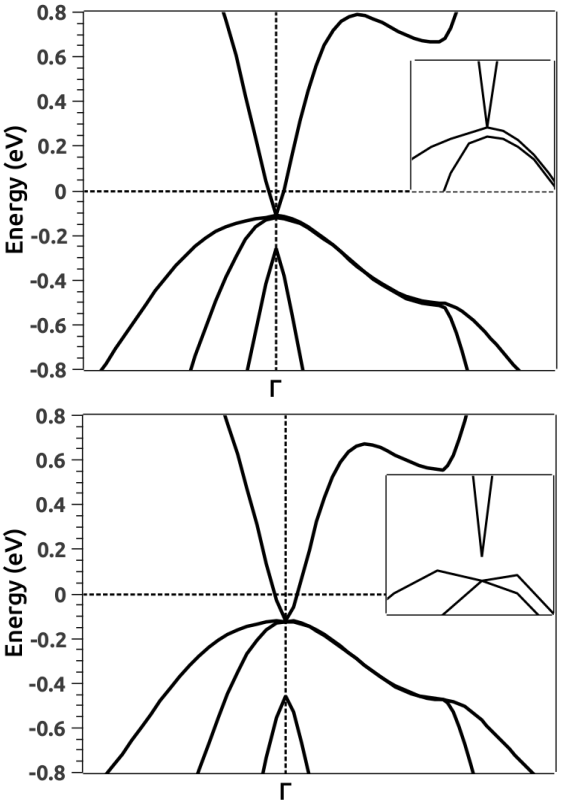


Figure 3.13: Electronic band structure at, 17% (top) and 20% (bottom) pressure indicating inversion of band dispersion.

Similar to LiMgBi and LiMgSb, LiMgAs exhibits semi-conducting character due to the 8-electron valency with indirect band gap as presented in Fig. 3.14. Since the zincblende sub-lattice formed by Mg-As in LiMgAs is adiabatically connected to the band topology

of HgTe, we discuss the topological properties in terms of band orders around Fermi level similar to that of HgTe i.e., the $\Gamma_8$ band denoting the p-type orbitals and $\Gamma_6$ band denoting the s-type orbitals. The band energies at these indices give insights into the band inversion strength which is given by $\Delta = E_{\Gamma_8} - E_{\Gamma_6}$.[26,46]

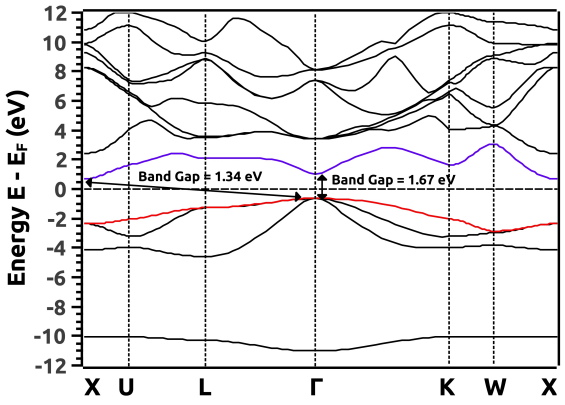


Figure 3.14: Electronic band structure of LiMgAs.

Although the global gap is of indirect nature along momentum path X → U → L → Γ in the brillouin zone, the system exhibits a direct gap of 1.67 eV at the brillouin zone center which is close to 1.55 eV observed in previous studies.[21] By applying volume expansion/compression pressure can drive the systems through a phase transition. We observed that, under volume compression the global gap increases indicting potential applications for strain induced photovoltaic's which is open for further research. However, our interest lies in a phase transition which would host Dirac degeneracy. This is observed under volume expansion pressure wherein contrary to compression; the applied pressure drives the system through a phase transition.

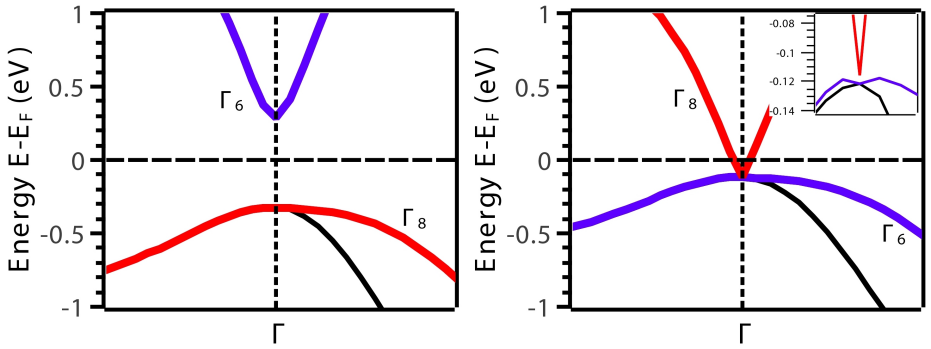


Figure 3.15: Electronic band structure around Fermi level indicating the Dirac degeneracy at critical pressure and band reopening at 17% pressure with dispersion inversion (right).

As the pressure is increased, the global gap becomes direct along the brillouin zone center and decreases as presented in Fig. 3.15(left). At 15% pressure, we observe the critical point of phase transition hosting the Dirac denegeracy as presented in Fig. 3.15(right). On increasing the pressure beyond this critical point, at 17% (inset Fig. 3.15(right)) the Dirac degeneracy lifts off indicating exchange of band dispersions. Apart from exchange of dispersions, we also

observe the exchange of orbitals as evident from the orbital projected density of states (with and without spin-orbit interactions) presented in Fig. 3.16. Under pristine conditions, the conduction band is populated by the *s*-orbitals arising from Li, Mg and As and the valence band populated purely by the *p*-orbitals arising from As.

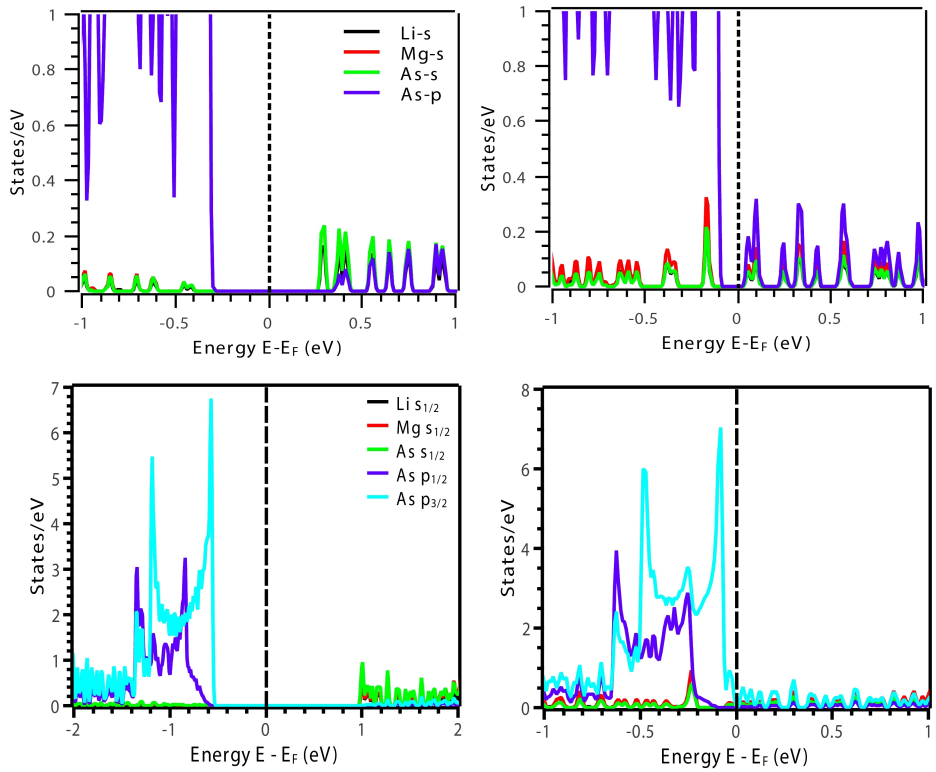


Figure 3.16: Orbital projected density of states without spin-orbit interactions (top) and with spin-orbit interactions (bottom) before (left) and at critical volume expansion pressure (right) respectively, hosting exchanged orbital features around Fermi.

The *s*-orbitals from Li, Mg and As exhibit strong hybridization with the *p*-orbitals of As in conduction band as compared to that in valence band. At the critical pressure the Dirac degeneracy leads to a non-negligible increase in the *p* and *s*-orbital contributions across the Fermi level is observed (as presented in Fig. 3.16(top)). As eviden from Fig. 3.16(top), the *s*-orbital contributions increase in the valence band but, the dominant contribution is from the *p*-orbital of As. This implies that, the inversion is weak owing to the presence of Fermions arising from the *p*-orbital of As. This leads to a linear Dirac dispersion in the conduction band and non-linear/parabolic dispersion in the valence band respectively. The corresponding velocity of Fermions was computed using, $v_f = \partial E/\hbar\partial k$.[47] We observed that, the velocity of Fermions in conduction band was, $\sim 0.06$ ms$^{-1}$ and $\sim 0.64$ ms$^{-1}$ along L $\rightarrow \Gamma$ and $\Gamma \rightarrow$ K directions in brillouin zone respectively. Similarly, in the valence band the velocity was, $\sim$

0.04 $ms^{-1}$ and $\sim$ 0.33 $ms^{-1}$ along L $\rightarrow \Gamma$ and $\Gamma \rightarrow$ K directions in brillouin zone respectively.

We also computed the band inversion strength ($\Delta$) which was quite weak i.e., $\Delta \sim 7.0$ meV. However, under spin-orbit interaction due to the high nuclear charge of As the Dirac degeneracy lifts off to $\sim$ 1.5 meV at the critical point in phase transition characterised by pronounced orbital exchanges as presented in Fig. 3.16(bottom). These qualitative computations were verified by quantitative computations of the topological porperties which gave a contradicting result.

## LiMgSb and LiMgAs: Topological Properties

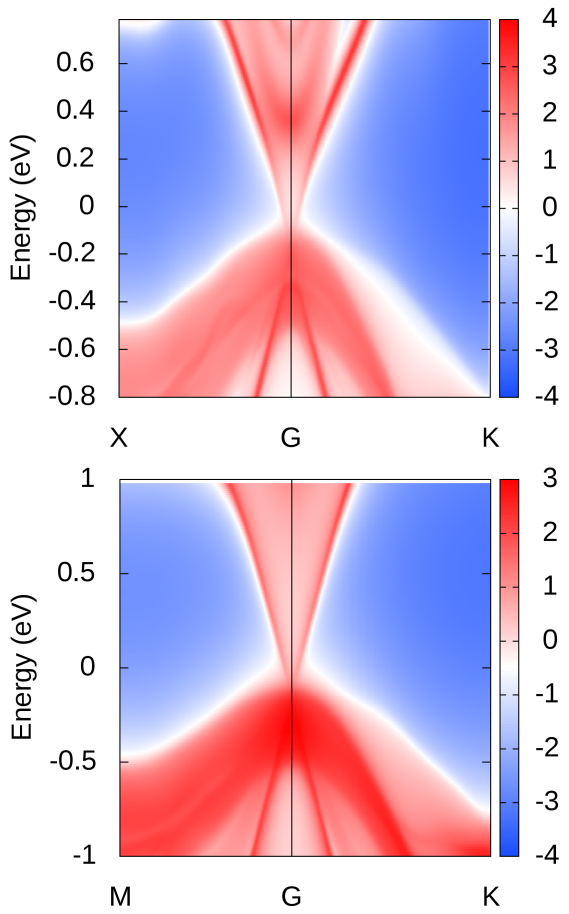


Figure 3.17: Angle resolved photoemission spectroscopy-like spectra of LiMgSb (top) and LiMgAs (bottom) beyond the critical pressure.

We observe that, both, LiMgSb and LiMgAs exhibit band dispersion inversions and exchange of orbital characters under the influence of volume expansion pressure as evident from our discussions above. Beyond the critical phase transition point, we computed the angle resolved photoemission spectroscopy-like spectra for LiMgSb and LiMgAs which are presented in Fig. 3.17 top and bottom panel respectively. These spectra do indicate that, the global bulk gap host conducting surface states. However, on computing the $\mathbb{Z}_2$ invariant (along the time reversal invariant points using the wannier charge center method) to classify the systems into non-trivial phases; we observed that, both LiMgSb and LiMgAs are trivial with $\mathbb{Z}_2$ invariants as $((\nu_0, \nu_1\nu_2\nu_3) = (0, 000))$ which contradicts our qualitative analysis. This implies that, the qualitative analysis of the electronic properties alone cannot be used to investigate the topological character of materials. Hence, computing the surface states along with the $\mathbb{Z}_2$ invariants are mandatory. This establishes a necessary and sufficient condition to

realise a toplogical insulator.

Such contradictory result originates from the fact that, the spin-orbit interactions due to Sb and As are far weaker as compared to Bi. Also, as evident from the electronic properties, the phase transtions in LiMgSb and LiMgAs occur at very high pressures, this implies that, we need to explore low dimensional phases which can be dimensionally engineered from these materials to realised non-trivial topological insulators at relative lower pressures due to high surface-to-volume ratio and quantum confinement effects. Potentially, the low dimensional phases engineered from these bulk materials can host topologically non-trivial behaviour as observed in HgTe which is trivial in bulk but non-trivial upon dimensional confinement. Also, as in LiMgBi, the Fermi level does not lie in the global gap hence we investigated alternate techniques such as the cubic symmetry is broken while realising the topological quantum phase transition. With this motivation, we explored binary compound AuI.

## 3.2 The Case of Binary Compound AuI

The beauty of non-trivial topological states lies in the exotic quantum phenomena observed in, topological conductors (where, the band bending leads to charge accumulation on surfaces) and topological insulators (wherein the bulk is insulating with conducting surfaces states robust against any sorts of perturbations).[1,3,48,70] The former has received scarce attention according to our literature survey while, the latter has gathered lots of attention in recent decades. Topological insulators are of a great interest because, these materials are also capable of hosting interesting properties with applications in, thermoelectrics, superconductivity etc.[5,20,49,50] Typically, in well explored topological insulators such as, $Bi_{(1-x)}Sb_x$, $Bi_2Te_3$, $Bi_2Se_3$, $Sb_2Te_3$, HgTe-CdTe etc.[24,51,52] the non-trivial topological states arise due to the band inversions across the Fermi level which exist due to strong spin-orbit interactions within the material due to heavy elements. Some of the most common orbital inversions protected by in ternal crystal symmetries and observed in topological quantum phase transitions are, *s-p* (in $Bi_{(1-x)}Sb_x$, HgTe-CdTe); *p-p* (in $Bi_2Te_3$, $Bi_2Se_3$, $Sb_2Te_3$) and *d-p* (in $IrBi_3$, LaAs).[24,51–54,70] In some cases, when a material exhibits weak spin-orbit interactions, it can be enhanced by applying strain/pressure which alters the orbital characters of the elements in the material.[19] In such scenarios, the band inversion mechanism is generally described as the closing and opening of conduction and valence band frontiers.[19,53] During such phase transitions the system traverses

through a critical point which exhibits Dirac degeneracy of the conduction and valence band frontiers along a high-symmetry point in the brillouin zone which is characterised as semi-metallic nature (analogous to the dispersions observed in two dimensional X-ene's).[55] Binary compounds such as, mercury chalcogenides (i.e., HgTe, HgSe, $\beta$-HgS) and wrutzite gold iodide (AuI) compounds are some classical examples of bulk semi-metallic materials.[12,56,57] Previously, binary compounds, HgTe, HgSe, AuI and Silver Iodide (AgI) were investigated for non-trivial topological states apart from their native semi-metallic character. It should be noted that, this semi-metallic nature is different from the one observed in topological Dirac semi-metals (or Weyl semi-metals). The latter exhibits degenerate nodes/points in the brillouin zone in the presence of spin-orbit interactions while the former does not possess degeneracies when the spin-orbit interactions are considered.[58]

Off these binary compopunds, AuI is an interesting candidate since it exists in different polymorphs. With its wrutzite phase explored for topological phenomena, the aurophilic tetragonal phase has been experimentally investigated under high-pressure.[56,59] With respect to topological properties, the wrutzite phase exhibits HgTe like inverted band structure with semi-metallic character. It is a fact that, wrutzite and zincblende crystal structures exhibit similar properties. This motivated us to explore topological quantum phenomena in zincblende phase of AuI since it had not been explored till date, due to debatable stability in the zincblende phase. Also, we were motivated to investigate AuI because of its similarity with HgTe (which exhibits topologial insulator nature when confined into quantum wells or under very high pressures in bulk phase).[60,61] With this motivation and background, we began our investigations on zincblende AuI by applying pressure. We found that, contrary to bulk HgTe and wrutzite AuI, the zincblende structure of AuI is highly sensitive to external perturbations and does not retain its the native semi-metallic character. Zincblende AuI undergoes topological quantum phase transitions when subjected to, (i) small isotropic compressive pressure and (ii) uni-axial pressure along [001] crystal direction breaking the cubic symmetry. Due to such high sensitivity, topological quantum phase transitions in AuI can be expected to occur at low pressures making it experimentally more feasible.

## AuI: Structure, Lattice Dynamics and Stability

The cubic zincblende structure of AuI belongs to the $F\bar{4}3m$[216] space group and $m\bar{3}m$ Laue class. It is basically a stuffing of $Au^{+1}$ and $I^{-1}$ ions as presented in Fig. 3.18. Such crystal

structure is governed by the bulk inversion asymmetry. Since, zincblende materials are non-centrosymmetric crystal structures without polar and chiral inversion centers, we can expect that, zincblende AuI would facilitate removal of band spin degeneracies due to spin-orbit interactions (which causes the coupling of electronic spin and orbital degrees of freedom) rather than external magnetic field. The governing dynamics of spin-orbit interactions in such systems originates from the asymmetry in the potential which favours unique spin orientations splitting the electronic bands into sub-bands which are spin aligned and anti-aligned. Under generalised gradient approximations, the optimized lattice constant (a) was found to be 6.54 Å. Since, zincblende AuI was predicted for the first time, we thoroughly investigate the structural stability and experimental viability in terms of energetic, mechanical and dynamic parameters. This was necessary because, there's a lot of debate in the condensed matter community regarding the stability of zincblende phase of AuI as compared to its wrutzite polymorph.

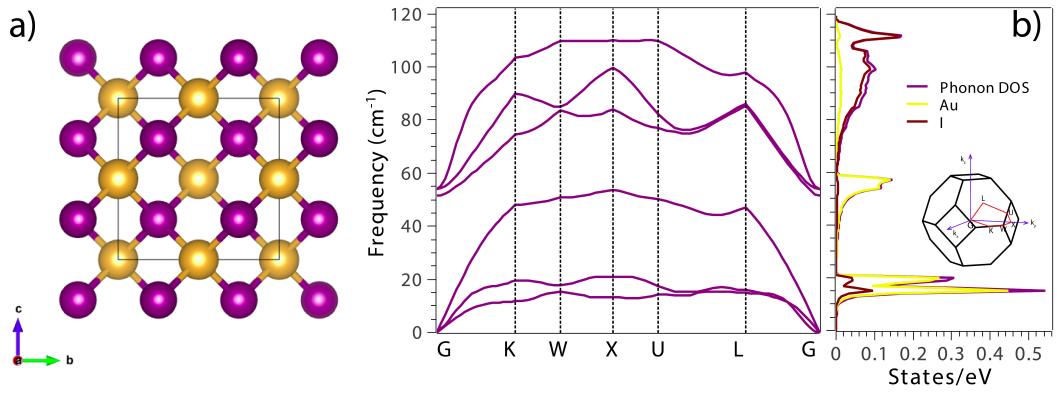


Figure 3.18: (a) Zincblende structure of AuI with, Au (golden) and I (purple) occupying two sublattice positions. (b) Phonon dispersion curves alongside the phonon density of states (inset brillouin zone).

Energetic stability gives insights into, whether the porposed system would be experimentally feasible based on thermodynamics. We compute the formation energy $\Delta E_f$ (defined as; $\Delta E_f = E_{AuI} - n_{Au}E_{Au} - n_I E_I$; where $E_X$ are the total energies) which can be used to predict the energetic stability of AuI. From a thermodynamic perspective, this gives insights into the type of reaction (endothermic or exothermic) which would lead to zincblende AuI. The criteria for a stable compound is that, the formation energy should be negative which indicates that, the end product is stable as compared to reactants. In case of zincblende AuI; the formation energy was found to be $\Delta E_f = -3.551$ eV/atom (since, $E_{AuI} = -1211.628$ eV/atom, $E_{Au} = -896.425$ eV/atom, $E_I = -311.652$ eV/atom, $n_{Au} = 1$ and $n_I = 1$). The negative formation energy implies that, zincblende AuI would form spontaneously when Au

and I are brough together.

To assess the practical applications of zincblende AuI we compute the mechanical properties which can be extracted by understanding the mechanical stability of the system. For this purpose, we compute second-order elastic tensors using first-principles total-energy and/or stress calculations. The elastic tensor matrix (with units in GPa) is presented below. Born and Huang established a criteria to predict the mechanical stability of materials in bulk and low dimensional phase in terms of elastic tensors. For a cubic system, these criteria are, $c_{11} - c_{12} > 0$, $c_{11} > 0$, $c_{44} > 0$ and $c_{11} + 2c_{12} > 0$ with $c_{11} > 0$ being an extra condition.[62] If the elastic tensors of a cubic material follow these criteria explicitly then, the material is said to be mechanically stable. These conditions are necessary and sufficient to indicate the stable or meta-stable configurations of materials.[63] As evident from the matrix above, the elastic tensors of AuI satisfy the Born-Huang criteria for cubic systems which indicates that zincblende AuI is mechanically stable. Apart stability, we also compute certain material properties using the elastic tensors. According to Pugh's criteria, Zincblende AuI exhibits ductile nature according to Pugh's criteria i.e., the ratio of shear modulus ($\mathcal{G} = 7.29$ GPa) to bulk modulus ($\mathcal{B} = 36.09$ GPa) is 0.20 which is $< 0.57$.[64] Also, zincblende AuI exhibits a youngs modulus of 20.49 GPa.[65] We use Lamé's relation to compute the Poisson's ratio which was found to be 0.41.[66] This value is comparable to isotropic engineering materials and polymers and in agreement with the ductile nature according to Pugh's criteria.[67]

$$\begin{bmatrix} C_{11} & C_{12} & C_{13} & 0 & 0 & 0 \\ C_{21} & C_{22} & C_{23} & 0 & 0 & 0 \\ C_{31} & C_{32} & C_{33} & 0 & 0 & 0 \\ 0 & 0 & 0 & C_{44} & 0 & 0 \\ 0 & 0 & 0 & 0 & C_{44} & 0 \\ 0 & 0 & 0 & 0 & 0 & C_{44} \end{bmatrix} = \begin{bmatrix} 41.2 & 33.5 & 33.5 & 0 & 0 & 0 \\ 33.5 & 41.2 & 33.5 & 0 & 0 & 0 \\ 33.5 & 33.5 & 41.2 & 0 & 0 & 0 \\ 0 & 0 & 0 & 11.2 & 0 & 0 \\ 0 & 0 & 0 & 0 & 11.2 & 0 \\ 0 & 0 & 0 & 0 & 0 & 11.2 \end{bmatrix}$$

To support the energetic and mechanical picture of stability, we compute the phonon dispersion curves which are essential to probe the lattice and vibrational dynamics of zincblende AuI eventually giving insights into the stability. From Fig. 3.18 it is clear that, the phonon dispersion curves and the phonon density of states do not possess negative vibrational frequencies throughout the brillouin zone; indicating dynamic stability of zincblende AuI. As compared to the half-heuslers discussed in previous section, due to two atoms in the unit cell of zincblende AuI we have six phonon branches which are distributed into three acoustic and

three optical modes. The acoustic modes account for the coherent motion of atoms whereas, the optical modes account for the incoherent motion of atoms. Since the zincblende AuI is ionic in nature we can expect that the optical modes would be IR active (since, the incoherent displacements would give rise to time-varying electric dipole moment). Experimentally, this feature can be exploited to characterize the proposed system.

## AuI: Electronic Properties

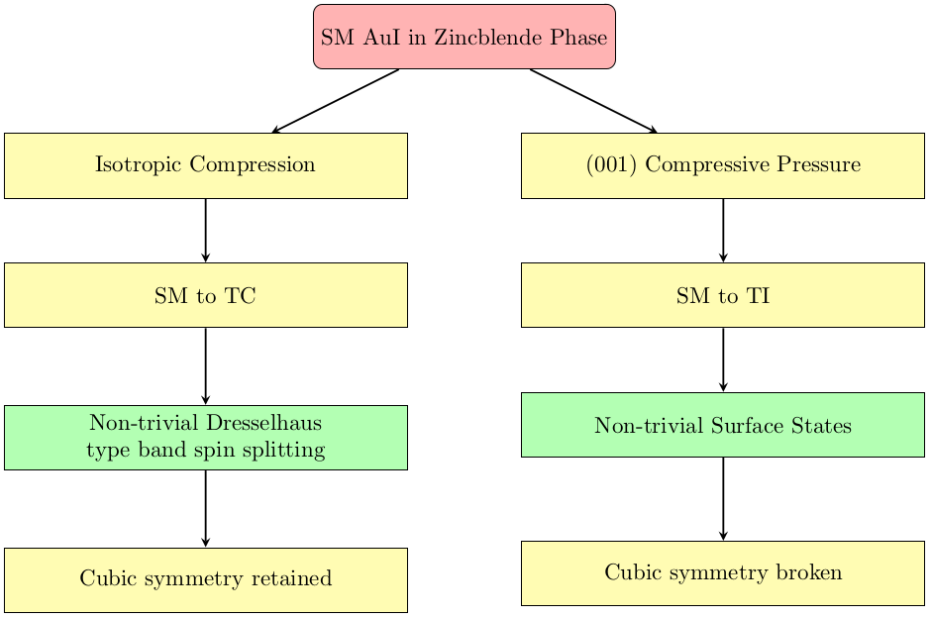


Figure 3.19: Flow chart indicating different approaches to realise non-trivial topological character in zincblende AuI. (left) Retaining cubic symmetry, under isotropic compression AuI undergoes topological phase transition from semi-metal to a topological conductor. (right) On breaking the cubic symmetry, under uni-axial compressive pressure (along [001] crystal direction) AuI undergoes topological phase transition from semi-metal to topological insulator.

Figure 3.19 presents different routes used to explore the topological quantum phase transitions in zincblende AuI. We found that, zincblende AuI exhibits anomalous behaviour as compared to its wrutzite polymorph, HgTe and other materials.[12,56,57] Under pristine conditions, zincblende AuI exhibits a semi-metallic nature, from here we follow two routes to realise non-trivial topological character. The first one (as presented in Fig. 3.19(left)) is, to impose isotropic compressive and expansive pressure on the system. On isotropic expansion we found that, the semi-metallic nature is lost which creates a global band gap making the system a trivial insulator which can be band engineered for ultra-wide opto-electronic applications. However, under isotropic compression, the system undergoes

non-trivial topological quantum phase transitions driving the semi-metallic system into a topological conducting state. Topological conductors exhibit Dresselhaus-like band-spin splitting governed by orbital band inversion.[68] Here, the Fermi level lies within the conduction band, hence to realise (a more desired) non-trivial topological insulating nature with the Fermi level lying in between the global gap we need to perform Fermi level engineering by varying the carrier concentrations.[48] However, if such approach is not feasible experimentally then, we can proceed with the second route (as presented in Fig. 3.19(right)). Here, we break the cubic symmetry by imposing a uni-axial compressive pressure along [001] crystal direction to realize a non-trivial topological quantum phase transition from semi-metal to topological insulator with Fermi level lying in between the global gap.[53] Both the routes are unique and governed by non-trivial topological band inversions involving *d*-orbitals originating from Au.[53]

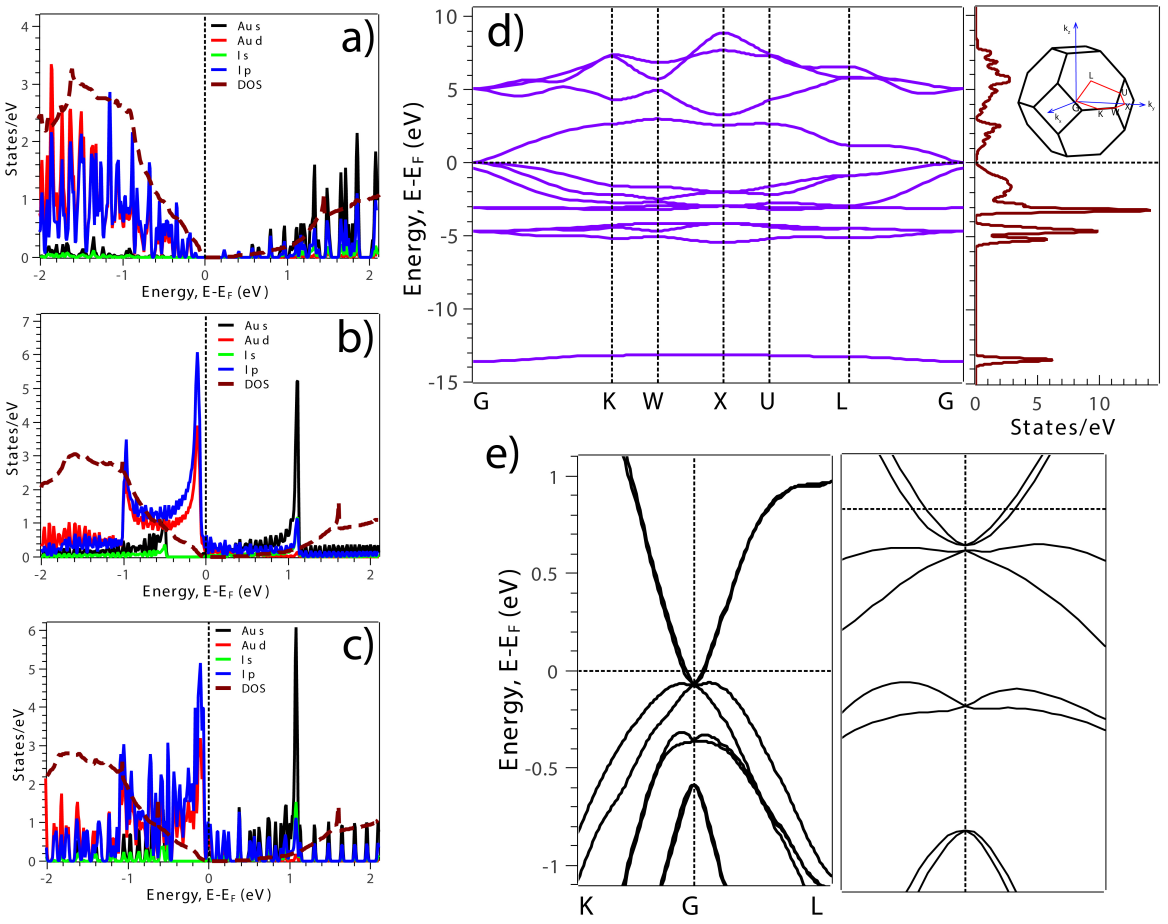


Figure 3.20: Orbital projected density of states (overlayed with density of states) at (a) 0%, (b) 0.5% and (c) 2% compressive pressures. (d) Electronic band structure alongside density of states showing semi-metallic nature at the center of brillouin zone (inset, momentum path). (e) Electronic band structure hosting, Dresselhaus-like band spin splitting and topological conducting state under 2% compressive pressure.

The electronic band structure of zincblende AuI exhibits Dirac denegeracies with degenerate conduction and valence band frontiers as presented in Fig. 3.20(d). As compared to wrutzite phase, the Dirac degeneracy is located at the brillouin zone center (Γ) with, *p*-orbitals of I and *d*-orbitals of Au populating the valence band and *s*-orbital of Au populating the conduction band (as presented in the orbital projected density of states at 0% pressure in Fig. 3.20(a)).[56] On imposing mild isotropic compressive pressure of 0.4%, AuI undergoes a topological quantum phase transitions from semi-metal to a non-trivial topological conductor with exchange of orbitals (as presented in the orbital projected density of states at 0.5% pressure in Fig. 3.20(b)).

Although, the Dirac degeneracy at the center of brillouin zone lifts off at around 0.2% only; but, the associated splitting is quite weak to realise a topological phase transition. Since appreciable splitting can be achieved under higher pressures we increased the pressure till 3% in steps of 0.2%. At 2% pressure, band splitting becomes quite prominent as presented in Fig. 3.20(e) which drives AuI into a non-trivial topological quantum phase transition. This non-trivial transition is accompanied by the exchange of orbital contributions across the Fermi level. Here, we observed a unique orbital inversion of *s* and *p-d* orbitals across the Fermi level as compared to other conventional invserions which involve on the *s* and/or *p*-orbitals. The band inversion is presented in Fig.3.20(c), in terms of the orbital projected density of states under 2% presented. Figure 3.20(e) presents the unique band-spin splitting Dresselhaus type. Such splitting originates due to the, non-centrosymmetric zincblende structure of AuI which is governed by bulk inversion asymmetry. The bulk inversion asymmetry gives rise to a perturbative Hamiltonian made up of odd powers of linear momentum ($p_i$, where $i$ = x, y, z) and pauli spin matrices ($\sigma_j$, where $j$ = x, y, z) as presented in Eq. 3.1 below.

$$H_D \propto p_x(p_y^2 - p_z^2)\sigma_x + p_y(p_z^2 - p_x^2)\sigma_y + p_z(p_x^2 - p_y^2)\sigma_z \tag{3.1}$$

The Fermi level enclosed in conduction band minima is a typical signature of a topological conductor (as evident from Fig. 3.20(e)) which is absent in the wrutzite phase of AuI.[56] The topological conducting nature originates from the band bending phenomena, hosting charge carrier accumulations on the surface. The anomalous downward band bending is quite common in several topological insulators owing to significant charge defects which alter the Fermi level in a material.[48] Hence, we can realise a non-trivial topological insulator from the topological conducting phase subjecting AuI to metal-insulator transition.[48] This can be

done by reducing the carrier concentrations governed by the Mott transition and Ioffe-Regel criterion (which requires increase in crystal disorder).[48] However, we can circum-navigate the requirement of engineering the Fermi level by breaking the cubic symmetry.

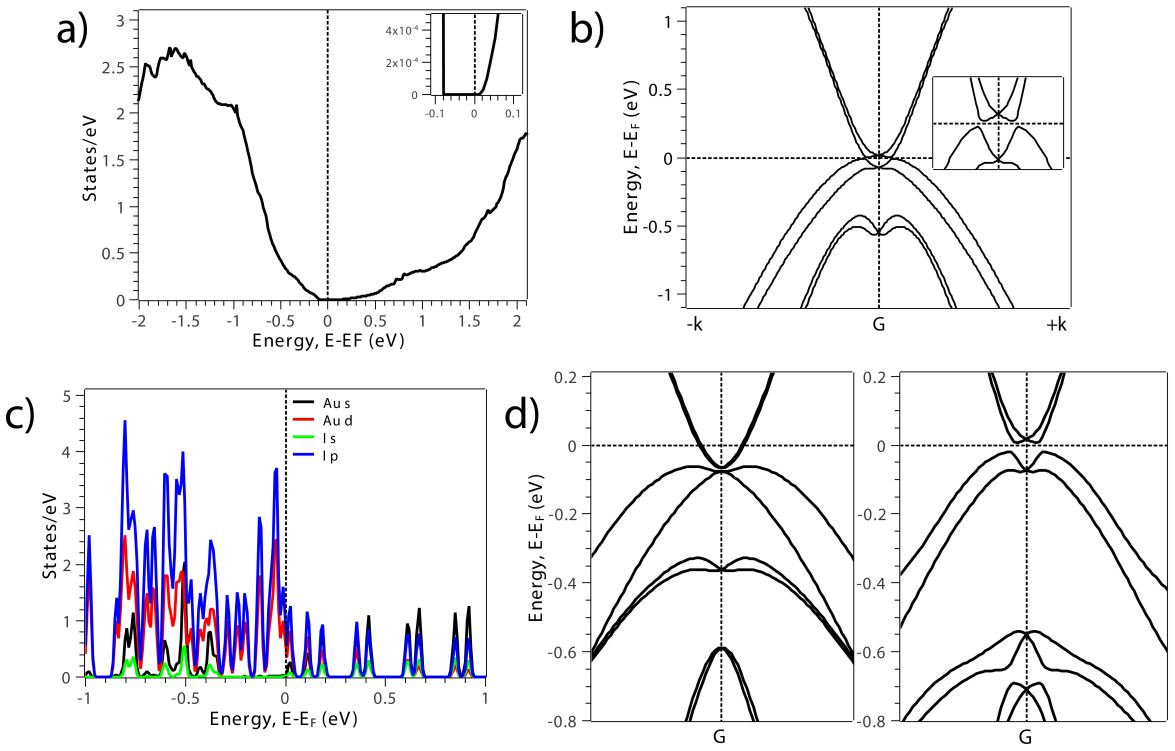


Figure 3.21: Density of states (a) and the electronic band structure (b) (with $\pm$ k = $\pm 2\pi$/a) at 1.1% uni-axial compressive pressure along [001] crystal direction (inset, indicates the non-trivial global band gap). (c) Orbital projected density of states indicating orbital exchange across the Fermi level. (d) Exact tight-binding model generated electronic band structure of AuI under 2% isotropic (left) and 1.1% uni-axial compression (right) respectively.

In case of semi-metallic cubic systems, it is well established in literature that, breaking the cubic symmetry would retain the orbital character of conduction and valence bands but lifts off the Dirac degeneracies at Fermi.[53] Hence, we subject the cubic zincblende AuI to uni-axial compressive pressure along [001] crystal direction which breaks the crystal cubic symmetry. As a result, this lifts off the Dirac degeneracies of the conduction and valence band frontiers at the center of the brillouin zone. In order a sizable gap we further increase the pressure from 0% to 2%. We come across a critical pressure at 1.1% which marks the non-trivial topological quantum phase transition.[14,53,69] This pressure is *critical* in the sense that, the valence band and conduction band are completely resolved across Fermi level (whereas, at 1.1 $\pm$ 0.1% the valence band crosses Fermi level) giving rise to a narrow global gap in the entire brillouin zone. This band opening at the critical pressure exhibits exchange of band

dispersions across Fermi level indicating band inversion as presented in Fig. 3.21(b). A global band gap of $\sim$ 79.84 meV was observed under the critical pressure as evident from the density of states and the electronic band structure presented in Fig. 3.21(a,b). This global band gap is narrow but superior as compared to other bulk topological insulators such as, $Sb_2Se_3$ and $\beta-As_2Te_3$.[14,69] On analysing the orbital projected density of states presented in Fig. 3.21(c) we find that, the orbital inversions as same as that in semi-metal to topological conductor transition. We compared the electronic band structure with the band structure obtained from the exact tight-binding hamiltonian and found that both the systems, under isotropic compressive pressure and uni-axial compressive pressure; host spin polarization as presented in Fig. 3.21(d). The unconventional and non-trivial topological properties observed in zincblende AuI can be attributed to the compressive pressure wherein the elements come closer, eventually enhancing the spin-orbit interactions originating from strong interactions between the atomic orbitals. Such a phenomena is known as proximity induced Kane-Mele interaction, which has been previously observed in two dimensional materials.[70]

## AuI: Topological Properties

Following the quantitatively analysis of non-trivial topological quantum phase transitions from; semi-metal to topological conductor and topological insulator, we now proceed with the quantitaive analysis in terms of the surface state spectra and the $\mathbb{Z}_2$ invariants. Since the system is cubic which lacks inversion symmetry, we employ the wannier charge center method to compute the $\mathbb{Z}_2$ invariants along the time reversal invariant planes. When the cubic symmetry is retained, the principle $\mathbb{Z}_2$ invariant $\nu_0$ changes from $\nu_0 = 0$ to $\nu_0 = 1$ (at 0.4% isotropic compression and beyond, till 3%). Similarly, when the cubic symmetry is broken under uni-axial pressure along [001] crystal direction, the $\mathbb{Z}_2$ invariants are $(\nu_0, \nu_1\nu_2\nu_3) = (1, 001)$ indicating that AuI is a strong topological insulator. Both the phases i.e., topological conductor and topological insulator are non-trivial and characterised by $\mathbb{Z}_2$ invariants. This is followed by computing the angle resolved photoemission spectroscopy-like spectra of the topological conductor and topological insulator which are presented in Fig. 3.22(a) and (b) respectively. Since the topological conductor obeys cubic symmetry the surface states are computed along the hexagonal surface which is evident from the brillouin zone path used in surface states (presented in Fig. 3.22(a)). However, when the cubic symmetry is broken the hexagonal surface losses its hexagonal symmetry hence, the brillouin zone path is presented in terms of

crystal momentum $\pm k$ (presented in Fig. 3.22(b)).

## 3.3 Conclusion

We presented our investigations of topological quantum phase transitions in bulk materials. We began with Half-Heusler compounds LiMgX (X = Bi, Sb, As); governed by $F\bar{4}3m$ space group with face centered cubic structures. LiMgBi was found to be dynamically stable with a direct global gap in the electronic band structure. On applying volume expansion pressure, we observed that at a critical pressure of 4.5% LiMgBi undergoes a topological quantum phase transition governed by *s-p* orbital band inversions with, spin-orbit coupling interactions induced gap of 1.10 meV. The closing and opening of the band gap was verified by using hybrid functional approach apart from the generalised gradient approach. The non-trivial character was verified by computing the surface state spectra which exhibit conducting nature. Also, we computed the $\mathbb{Z}_2$ invariants which were $(\nu_0, \nu_1\nu_2\nu_3) = (1, 0\,0\,0)$ which indicated that, LiMgBi is a strong topological insulator. We then presented similar phase transitions in LiMgSb, however, we observed that although LiMgSb presented band gap closing and reopening alongwith exchange of orbitals across Fermi level and conducting surface state spectra but, on computing the $\mathbb{Z}_2$ invariants we found it to be a trivial insulator. Similarly, LiMgAs which was another direct band gap semi-conductor was subjected to pressure. Similar to LiMgSb, this system also presented band gap closing and reopening with exchange of orbital characters across Fermi level and conducting surface state spectra, but on computing the $\mathbb{Z}_2$ invariants we found it to be a trivial insulator like LiMgSb. Although the site 'X' in LiMgX were replaced with members of pnictogen family but, we observed contradicting topological properties. With this

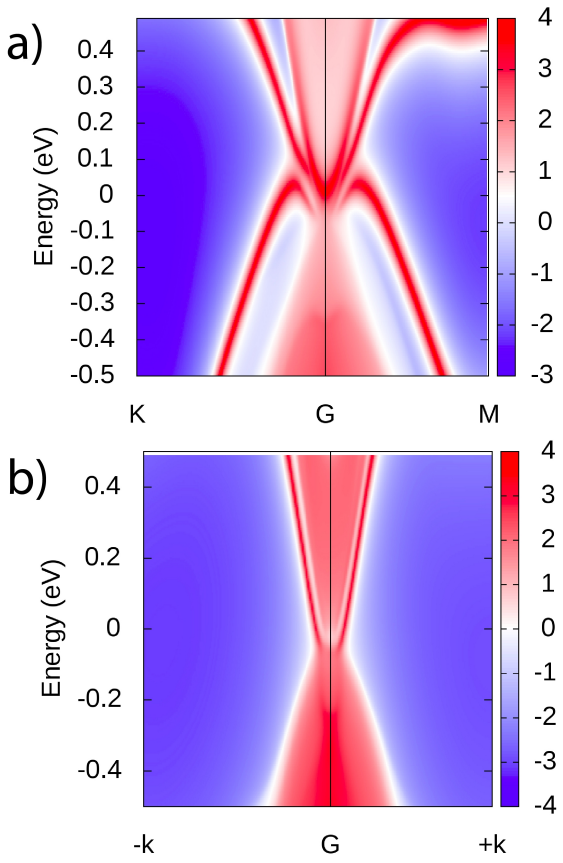


Figure 3.22: Angle resolved photoemission spectroscopy-like spectra of AuI indicating surface states in (a) topological conducting phase and (b) topological insulating phase.

we established the necessary and sufficient condition for realising a non-trivial topological insulator i.e., apart from band gap closing and reopening, orbital inversion across Fermi level and conducting surface state spectra, the system should *necessarily* exhibit non-trivial $\mathbb{Z}_2$ invariants. Further, since these systems (LiMgSb, and LiMgAs) presented topological phase transitions at very high pressures we proposed that, dimensionally engineered monolayers can be realised using these bulk materials to realise non-trivial topological quantum phase transitions at relatively lower pressures.

Another problem in the topological insulator LiMgBi was that, the conduction bands crossed the Fermi level during the topological phase transitions. We addressed this issue by breaking the cubic symmetry and converting the material from a topological conductor to a topological insulator. We presented this phenomena in binary zincblende compound AuI. Although the stability of such a compound has been debated but, on computing phonon dispersion curves, formation energy and elastic tensors we found that, AuI is dynamically, energetically and mechanically stable. We followed two approaches to realise non-trivial topological properties in this binary compound, (i) application of isotropic ompression and (ii) application of uni-axial compressive pressure along [001] crystal direction. We observed semi-metal to topological conductor and topological insulator transitions respectively under the said approaches. We observed that, due to the bulk inversion asymmetry, AuI exhibits Dresselhaus-like band-spin splittings characterized by unconventional *s*, *p-d* orbital band inversions. The non-trivial nature was confirmed by computing the conducting surface state spectra and the principle $\mathbb{Z}_2$ invariant which was $\nu_0 = 1$ (when cubic symmetry was retained and broken).

# Bibliography

[1] Joel E. Moore.Nature, 464(7286):194–198, Mar 2010.

[2] Liang Fu, Charles L Kane, and Eugene J Mele.Physical review letters, 98(10):106803, 2007.

[3] M Zahid Hasan and Charles L Kane.Reviews of modern physics, 82(4):3045, 2010.

[4] M. Zahid Hasan and Joel E. Moore.Annual Review of Condensed Matter Physics, 2(1):55–78, 2011.

[5] Xiao-Liang Qi and Shou-Cheng Zhang.Reviews of Modern Physics, 83(4):1057, 2011.

[6] Yoichi Ando.Journal of the Physical Society of Japan, 82(10):102001, 2013.

[7] WanXiang Feng and YuGui Yao.Science China Physics, Mechanics and Astronomy, 55(12):2199–2212, 2012.

[8] Peng-Jie Guo, Huan-Cheng Yang, Kai Liu, and Zhong-Yi Lu.Physical Review B, 96(8):081112, 2017.

[9] Jing-Yang You, Xue-Juan Dong, Bo Gu, and Gang Su.Physical Review B, 103(10):104403, 2021.

[10] Kyung-Hwan Jin, Han Woong Yeom, and Feng Liu.Physical Review B, 101(3):035111, 2020.

[11] Honghao Yao and Chen Chen and Wenhua Xue and Fengxian Bai and Feng Cao and Yucheng Lan and Xingjun Liu and Yumei Wang and David J. Singh and Xi Lin and Qian Zhang, Science Advances, 7(6), eabd6162, 2021.

[12] Lars Winterfeld, Luis A Agapito, Jin Li, Nicholas Kioussis, Peter Blaha, and Yong P Chen.Physical Review B, 87(7):075143, 2013.

[13] T Hirahara, N Fukui, T Shirasawa, M Yamada, M Aitani, H Miyazaki, M Matsunami, S Kimura, T Takahashi, S Hasegawa, et al.Physical review letters, 109(22):227401, 2012.

[14] Koushik Pal and Umesh V Waghmare.Applied Physics Letters, 105(6):062105, 2014.

[15] Shi Liu, Youngkuk Kim, Liang Z Tan, and Andrew M Rappe.Nano Letters, 16(3):1663–1668, 2016.

[16] Heejun Yang, Sung Wng Kim, Manish Chhowalla, and Young Hee Lee.Nature Physics, 13(10):931–937, 2017.

[17] Junwei Liu, Hua Wang, Chen Fang, Liang Fu, and Xiaofeng Qian.Nano Letters, 17(1):467–475, 2017.

[18] H Aramberri and MC Munoz.Journal of Physics: Materials, 1(1):015009, 2018.

[19] Luis A Agapito, Nicholas Kioussis, William A Goddard III, and Nai Phuan Ong, Physical review letters, 110(17):176401, 2013.

[20] F Casper, T Graf, S Chadov, B Balke, and C Felser.Semiconductor Science and Technology, 27(6):063001, 2012.

[21] Anindya Roy, Joseph W Bennett, Karin M Rabe, and David Vanderbilt.Physical review letters, 109(3):037602, 2012.

[22] Manoj K Yadav and Biplab Sanyal.Journal of Alloys and Compounds, 622:388–393, 2015.

[23] Bartomeu Monserrat, Joseph W Bennett, Karin M Rabe, and David Vanderbilt.Physical review letters, 119(3):036802, 2017.

[24] Haijun Zhang, Chao-Xing Liu, Xiao-Liang Qi, Xi Dai, Zhong Fang, and Shou-Cheng Zhang.Nature physics, 5(6):438–442, 2009.

[25] Hem Chandra Kandpal, Claudia Felser, and Ram Seshadri.Journal of Physics D: Applied Physics, 39(5):776, 2006.

[26] Arun Bansil, Hsin Lin, and Tanmoy Das.Reviews of Modern Physics, 88(2):021004, 2016.

[27] PC Canfield, JD Thompson, WP Beyermann, A Lacerda, MF Hundley, E Peterson, Z Fisk, and HR Ott.Journal of applied physics, 70(10):5800–5802, 1991.

[28] Hsin Lin, L Andrew Wray, Yuqi Xia, Suyang Xu, Shuang Jia, Robert J Cava, Arun Bansil, and M Zahid Hasan.Nature materials, 9(7):546–549, 2010.

[29] Stanislav Chadov, Xiaoliang Qi, Jurgen Kubler, Gerhard H Fecher, Claudia Felser, and Shou Cheng Zhang.Nature materials, 9(7):541–545, 2010.

[30] Wael Al-Sawai, Hsin Lin, RS Markiewicz, LA Wray, Y Xia, S-Y Xu, MZ Hasan, and A Bansil.Physical Review B, 82(12):125208, 2010.

[31] Joseph Bennett.Bull. Am. Phys. Soc, 58, 2013.

[32] T Suzuki, R Chisnell, A Devarakonda, Y-T Liu, W Feng, D Xiao, Jeffrey W Lynn, and JG Checkelsky.Nature Physics, 12(12):1119–1123, 2016.

[33] A Amudhavalli, R Rajeswarapalanichamy, K Iyakutti, and AK Kushwaha.Computational Condensed Matter, 14:55–66, 2018.

[34] Shi-Yuan Lin, Ming Chen, Xiao-Bao Yang, Yu-Jun Zhao, Shu-Chun Wu, Claudia Felser, and Binghai Yan.Physical Review B, 91(9):094107, 2015.

[35] Jianghui Liu, Guohua Cao, Zizhen Zhou, and Huijun Liu.Journal of Physics: Condensed Matter, 33(32):325501, 2021.

[36] Feng, Wanxiang and Zhu, Wenguang and Weitering, Hanno H and Stocks, G Malcolm and Yao, Yugui and Xiao, Di, Physical Review B, 85(19), 195114, 2012.

[37] Eric Herbert, Sebastien Balibar, and Frederic Caupin.Physical Review E, 74(4):041603, 2006.

[38] Gang Chen.Nanoscale energy transport and conversion: a parallel treatment of electrons, molecules, phonons, and photons. Oxford university press, 2005.

[39] Alec Belsky, Mariette Hellenbrandt, Vicky Lynn Karen, and Peter Luksch.Acta Crystallographica Section B: Structural Science, 58(3):364–369, 2002.

[40] Wanxiang Feng, Di Xiao, Jun Ding, and Yugui Yao.Physical review letters, 106(1):016402, 2011.

[41] Duane C Wallace.American Journal of Physics, 40(11):1718–1719, 1972.

[42] Martin T Dove and Martin T Dove.Introduction to lattice dynamics. Number 4. Cambridge university press, 1993.

[43] Atsushi Togo and Isao Tanaka.Scripta Materialia, 108:1–5, 2015.

[44] Prafulla K Jha and Sankar P Sanyal.Physica C: Superconductivity, 271(1-2):6–10, 1996.

[45] Sanjay D Gupta, Sanjeev K Gupta, Prafulla K Jha, and NN Ovsyuk.Journal of Raman Spectroscopy, 44(6):926–933, 2013.

[46] Kulwinder Kaur, Shobhna Dhiman, and Ranjan Kumar.Physics Letters A, 381(4):339–343, 2017.

[47] Zhongfei Liu, Peihong Wang, Qiaoyu Cui, Guang Yang, Shaowei Jin, and Kuangwei Xiong.RSC advances, 9(5):2740–2745, 2019.

[48] Matthew Brahlek, Nikesh Koirala, Namrata Bansal, and Seongshik Oh.Solid State Communications, 215:54–62, 2015.

[49] Ryuji Takahashi and Shuichi Murakami.Semiconductor Science and Technology, 27(12):124005, 2012.

[50] Yuri V Ivanov, Alexander T Burkov, and Dmitry A Pshenay-Severin.physica status solidi (b), 255(7):1800020, 2018.

[51] B Andrei Bernevig, Taylor L Hughes, and Shou-Cheng Zhang.science, 314(5806):1757–1761, 2006.

[52] Markus Konig, Steffen Wiedmann, Christoph Brune, Andreas Roth, Hartmut Buhmann, Laurens W Molenkamp, Xiao-Liang Qi, and Shou-Cheng Zhang.Science, 318(5851):766–770, 2007.

[53] Ming Yang and Wu-Ming Liu.Scientific reports, 4(1):1–7, 2014.

[54] Shoaib Khalid, Fernando P Sabino, and Anderson Janotti.Physical Review B, 98(22):220102, 2018.

[55] Aidi Zhao and Bing Wang.APL Materials, 8(3):030701, 2020.

[56] XM Zhang, RS Ma, XC Liu, GZ Xu, EK Liu, GD Liu, ZY Liu, WH Wang, and GH Wu, Europhysics Letters, 103(5):57012, 2013.

[57] Daniel Dumett Torres, Progna Banerjee, Sudhakar Pamidighantam, and Prashant K Jain.Chemistry of Materials, 29(15):6356–6366, 2017.

[58] Hongming Weng, Xi Dai, and Zhong Fang.Journal of Physics: Condensed Matter, 28(30):303001, 2016.

[59] Emanuele Priola, Nadia Curetti, Domenica Marabello, Jacopo Andreo, Alessia Giordana, Luca Andreo, Piera Benna, Paulo Tarso Cavalcante Freire, Paola Benzi, Lorenza Operti, et al.CrystEngComm, 24(12):2336–2348, 2022.

[60] Dimitrie Culcer, Aydin Cem Keser, Yongqing Li, and Grigory Tkachov.2D Materials, 7(2):022007, mar 2020.

[61] Jiawei Ruan, Shao-Kai Jian, Hong Yao, Haijun Zhang, Shou-Cheng Zhang, and Dingyu Xing.Nature communications, 7(1):1–6, 2016.

[62] Max Born and Kun Huang.Dynamical theory of crystal lattices. Oxford University Press, 1954.

[63] Felix Mouhat and Francois-Xavier Coudert.Physical review B, 90(22):224104, 2014.

[64] SF Pugh.The London, Edinburgh, and Dublin Philosophical Magazine and Journal of Science, 45(367):823–843, 1954.

[65] Richard Hill.Proceedings of the Physical Society. Section A, 65(5):349, 1952.

[66] PH Mott and CM Roland.Physica Scripta, 87(5):055404, 2013.

[67] PH Mott and CM Roland.Physical review B, 80(13):132104, 2009.

[68] Xin Liu, Xiong-Jun Liu, and Jairo Sinova.Physical Review B, 84(3):035318, 2011.

[69] Wenliang Liu, Xiangyang Peng, Chao Tang, Lizhong Sun, Kaiwang Zhang, and Jianxin Zhong.Physical Review B, 84(24):245105, 2011.

[70] Liangzhi Kou, Feiming Hu, Binghai Yan, Thomas Frauenheim, and Changfeng Chen, Nanoscale, 6(13):7474–7479, 2014.